# Layer-specific network oscillation and spatiotemporal receptive field in the visual cortex

**Wenzhi Sun and Yang Dan[1]**

Howard Hughes Medical Institute, Department of Molecular and Cell Biology, University of California, Berkeley, CA 94720

Edited by Charles F. Stevens, The Salk Institute for Biological Studies, La Jolla, CA, and approved August 31, 2009 (received for review April 10, 2009)

**A quintessential feature of the neocortex is its laminar organization, and characterizing the activity patterns in different layers is an important step in understanding cortical processing. Using in vivo whole-cell recordings in rat visual cortex, we show that the temporal patterns of ongoing synaptic inputs to pyramidal neurons exhibit clear laminar specificity. Although low-frequency (~2 Hz) activity is widely observed in layer 2/3 (L2/3), a narrow-band fast oscillation (10–15 Hz) is prominent in layer 5 (L5). This fast oscillation is carried exclusively by excitatory inputs. Moreover, the frequency of ongoing activity is strongly correlated with the spatiotemporal window of visual integration: Neurons with fast-oscillating spontaneous inputs exhibit transient visual responses and small receptive fields (RFs), whereas those with slow inputs show prolonged responses and large RFs. These findings suggest that the neural representation of visual information within each layer is strongly influenced by the temporal dynamics of the local network manifest in spontaneous activity.**

lamina | ongoing activity | patch clamp | pyramidal cell | vision

Coherent oscillatory activity in neuronal populations has been widely observed in the nervous system. Studies in both humans and animal models have shown that oscillations in various frequency bands are correlated with the behavioral or attentional state of the subject (1–5). The synchronization of activity within an oscillating ensemble and the temporal phase of single neuron spiking relative to the network oscillation may be used to carry sensory information (6–9), to control synaptic interactions (10), or to regulate activity-dependent synaptic modification (2, 11, 12). Thus, network oscillations may be involved in a range of essential brain functions.

To elucidate the function of a given type of oscillation, it is important to know which neurons participate in the oscillating ensemble. In the neocortex, the spatial extent of coherent oscillation has been studied extensively along the cortical surface (4–6, 13). However, little is known about the laminar distribution of oscillations in the intact brain. The laminar organization of cortical microcircuit plays crucial roles in information processing. Neurons in different layers exhibit different synaptic connectivity, and the representation of sensory signals is transformed systematically across layers (14, 15). Thus, an important question is whether oscillations show any laminar specificity, and whether layer-specific oscillations contribute to cortical processing.

In the current study, we used in vivo whole-cell recordings to measure both the spontaneous activity and the spatiotemporal receptive fields (RFs) of rat visual cortical neurons. We found that pyramidal neurons in L2/3 and L5 exhibit distinct patterns of membrane potential oscillations in the absence of visual input, whereas L2/3 neurons exhibit slow spontaneous activity at ≈2 Hz, reflecting both excitatory and inhibitory inputs, L5 neurons show a strong oscillation at 10–15 Hz driven exclusively by excitatory inputs. Furthermore, the spontaneous oscillation patterns are closely related to the visual response properties of these neurons. While the low-frequency neurons exhibit slower visual responses and larger RFs, the fast-oscillating neurons show transient visual responses and smaller RFs. The layer-specific oscillations appear to gate the spatiotemporal integration of visual information and thus contribute to the distinct function of each layer in cortical processing.

## Results

Patch-clamp recordings were made from 127 neurons in the primary visual cortex of anesthetized adult rats using the conventional whole-cell or perforated patch technique (*Materials and Methods*). The spiking patterns of these cells in response to depolarizing current injection suggested that they were excitatory neurons. Histological reconstruction of a subset of the cells labeled with neurobiotin ($n = 20$) confirmed that they were pyramidal neurons (Figs. 1 *A* and *D* and 2 *A* and *D*).

**Layer-Specific Spontaneous Activity.** In the absence of visual stimulation, we found a high level of spontaneous activity in the recorded neurons. Fig. 1 *A* and *D* show two reconstructed pyramidal neurons in L2/3. Recordings under voltage clamp at −70 mV revealed large inward synaptic currents occurring at a frequency of 1–6 events/s with peak amplitudes of 80–500 pA and durations of a few hundred milliseconds (Fig. 1 *B* and *E Upper*). Under current clamp, the spontaneous activity manifests as membrane depolarization events with amplitudes of 5–30 mV (*Lower*), sometimes leading to spikes. The large amplitudes of these synaptic events suggest that they did not result from spontaneous spiking of a single presynaptic neuron, which evokes excitatory postsynaptic potentials (EPSPs) on the order of 1 mV (16); instead they reflect coordinated activation of a population of neurons connected to the recorded cell. The power spectra of the spontaneous currents showed an overall decrease at high frequencies (Fig. 1 *C* and *F*). For many cells, there was a prominent peak at ≈2 Hz (Fig. 1*C*), reflecting quasi-periodicity of the spontaneous events.

The pyramidal cells in L5 (Fig. 2 *A* and *D*), however, exhibited very different patterns of spontaneous activity. Both current- and voltage-clamp recordings revealed prominent high-frequency synaptic events with shorter durations (Fig. 2 *B* and *E*). The amplitudes of these events were comparable to those found in L2/3 cells (Fig. 1), suggesting that they also resulted from coordinated spiking of a population of presynaptic neurons. The power spectrum of spontaneous activity showed a prominent peak at 10–15 Hz (Fig. 2 *C* and *F*), with the narrowness of the peak reflecting a high degree of periodicity of these events. In addition to the fast oscillation, we also observed some long-duration, low-frequency synaptic events (Fig. 2 *B* and *E*) that were similar to those found in L2/3. Fig. 3*A* shows the average power spectra of all of the reconstructed neurons in L2/3 (*Upper*, $n = 8$) and L5 (*Lower*, $n = 12$). Although the peak at ≈2 Hz, reflecting the slow synaptic events, is present for both populations of neurons (although more prominent in L2/3), the peak at 10–15 Hz is found only in L5. This observation suggests that

Author contributions: W.S. and Y.D. designed research; W.S. performed research; W.S. and Y.D. analyzed data; and W.S. and Y.D. wrote the paper.

The authors declare no conflict of interest.

This article is a PNAS Direct Submission.

[1]To whom correspondence should be addressed. E-mail: ydan@berkeley.edu.

This article contains supporting information online at www.pnas.org/cgi/content/full/0903962106/DCSupplemental.

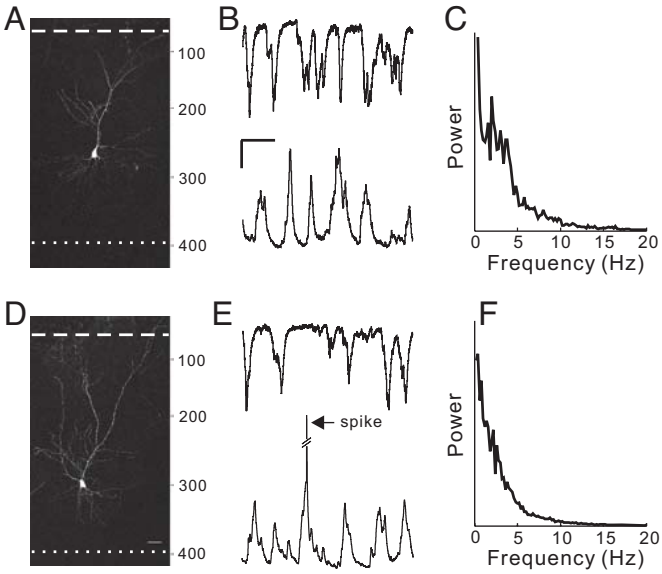


**Fig. 1.** Spontaneous synaptic inputs to L2/3 pyramidal neurons. (*A*) Fluorescence image of an example cell. Numbers, distances from pia in $\mu$m. Dashed and dotted lines, estimated upper and lower borders of L2/3. (*B*) Example current (*Upper*) and voltage (*Lower*) traces recorded under voltage and current clamp, respectively. (Scale bars: 500 ms, 50 pA/5 mV.) (*C*) Power spectrum of spontaneous currents. (*D–F*) Same as *A–C* for another L2/3 neuron.

the slow network activity is distributed across layers, whereas the fast oscillation is restricted to L5.

To quantify the laminar distribution of the cells exhibiting 10–15 Hz spontaneous oscillation, for each cell we measured the power ratio of spontaneous currents, defined as $(P_{high} - P_{low})/(P_{high} + P_{low})$ ($P_{high}$ and $P_{low}$ represent the power in the 10–20 Hz and 5–10 Hz ranges, respectively, Fig. 3*B*). Fig. 3*C* summarizes the relationship between the power ratio and the cortical depth of the recording electrode (estimated by the distance traveled from cortical surface) for 76 neurons. The fast-oscillating neurons (with high power ratios) are located predominantly in deep layers, supporting our finding based on the subset of reconstructed cells (■, L2/3; ▼, L5).

To ensure that the different activity patterns found in these layers were not due to changes in the overall brain state, we made simultaneous recordings in L2/3 and L5 with a local field potential (LFP) electrode paired with a whole-cell or another LFP electrode. The spontaneous activity in L5 exhibited higher frequencies than that in L2/3 in all simultaneous recordings ( Fig. S1), and the peak at 10–15 Hz was found in whole-cell recordings from L5 (Fig. S1 *B* and *C*), but not from L2/3 (Fig. S1*E*) neurons, indicating that the difference is not because of changes in brain state. A difference between LFP and whole-cell recordings is that the 10–15 Hz oscillation prominent in L5 intracellular signals (Fig. S1 *B* and *C*) was not evident in the LFP (Fig. S1 *E*, *G*, and *H*), suggesting that this oscillation is not phase-synchronized over the spatial scale sampled by LFP recordings (several hundred micrometers).

To test whether the observed laminar difference is restricted to pentobarbital anesthesia, we also made whole-cell recordings under urethane. Compared with L2/3 neurons (Fig. S2 *A–C*), L5 neurons again exhibited higher-frequency spontaneous activity with a narrow-band oscillation (Fig. S2 *D–F*), although the oscillation frequency was approximately half of that found under pentobarbital anesthesia. The power ratio between 5–10 Hz and 2.5–5 Hz (Fig. S2*G*, chosen based on the L5 oscillation frequency) increased significantly with cortical depth (Fig. S2*H*, $P < 0.01$). Thus, although there were quantitative differences between the two anesthetics, the laminar difference in spontaneous activity was robust under both conditions.

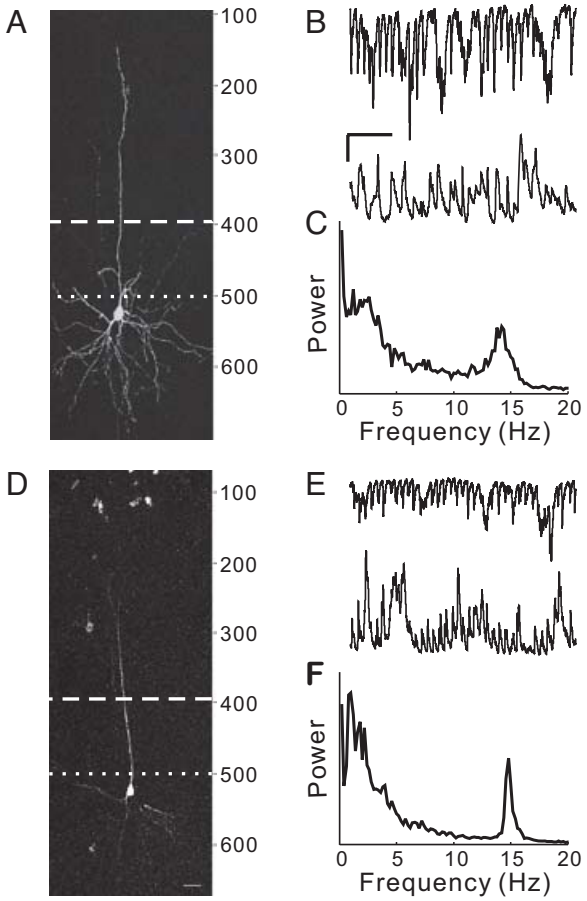


**Fig. 2.** Spontaneous synaptic inputs to L5 pyramidal neurons. (*A*) Fluorescence image of an example L5 neuron. Dashed and dotted lines, estimated borders of L4. (*B*) Example current (*Upper*) and voltage (*Lower*) traces recorded under voltage and current clamp, respectively. (Scale bars: 500 ms, 50 pA/5 mV.) (*C*) Power spectrum of spontaneous currents. (*D–F*) Same as *A–C* for another L5 neuron.

**Fast Oscillation Is Mediated by Excitatory Inputs.** Previous studies suggest that synchronous oscillations in the gamma band (30–80 Hz) depend on activity of the inhibitory interneurons (17–21). Here, to estimate the excitatory and inhibitory components of the spontaneous synaptic activity, we made recordings from each cell at multiple holding potentials between −100 and 0 mV. For L2/3 neurons, the amplitudes of inward currents were reduced at depolarized potentials, and outward currents were clearly detectable near 0 mV (Fig. 4*A*). The existence of inward currents at 0 mV (reversal potential for excitatory inputs) suggests that at least some of the excitatory inputs are from distal dendrites, whereas the local membrane potential may be much more hyperpolarized than the holding potential at the cell body (see *Discussion*). Nevertheless, power spectral analysis showed that holding the cell at 0 mV caused a marked reduction of the peak at ≈2 Hz and an increase of power at higher frequencies (Fig. 4*B*). This finding suggests that whereas the excitatory inputs are quasi-periodic at ≈2 Hz, the inhibitory inputs contain more power at high frequencies (20).

For L5 neurons, the fast and slow components of the spontaneous activity exhibited different dependence on the holding potential (Fig. 4*C*). When the cell was held at more depolarized potentials, the slower events changed from purely inward to bidirectional, similar to those found in L2/3 (Fig. 4*A*). However, the fast oscillatory inward currents diminished in amplitude without reversing polarity. As shown in the power spectra in Fig. 4*D*, the peak at 10–15 Hz was largely eliminated at 0 mV, indicating that the

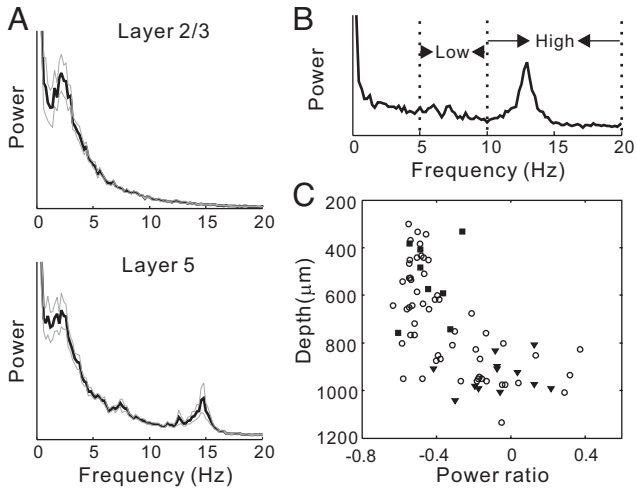


**Fig. 3.** Dependence of spontaneous activity pattern on cortical depth. (*A*) Power spectra of spontaneous synaptic currents averaged from 8 reconstructed L2/3 neurons (*Upper*) and 12 reconstructed L5 neurons (*Lower*). The spectrum of each cell was normalized by the mean power density at 5–10 Hz. Thick line, mean; thin lines, ± SEM. (*B*) Definition of "high" and "low" frequency ranges for computing power ratio. Shown is power spectrum of an example L5 neuron. The high frequency range (10–20 Hz) is chosen to include the 10–15 Hz peak. (*C*) Cortical depth estimated from distance traveled by electrode vs. power ratio. The correlation is highly significant ($P < 10^{-9}$). Filled symbols: reconstructed cells (■, L2/3; ▼, L5).

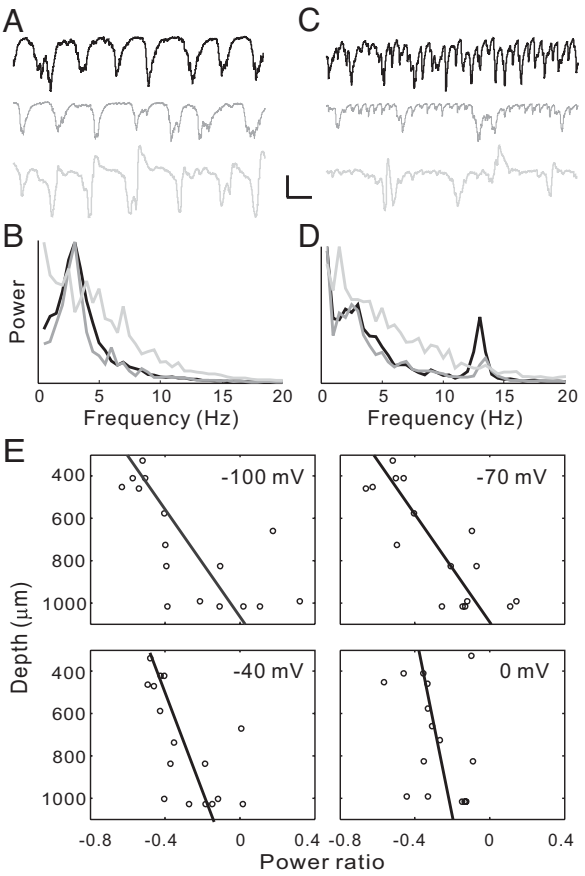


**Fig. 4.** Dependence of spontaneous synaptic current on holding potential. (*A*) Spontaneous synaptic currents recorded from a L2/3 neuron held at −100 (black), −70 (dark gray), and 0 (light gray) mV. (Scale bars: 250 ms; 200 pA.) (*B*) Power spectra of currents recorded at the three holding potentials. (*C*) Same as *A* for a L5 neuron. (Scale bars: 250 ms; 400 pA.) (*D*) Same as *B* for the cell in *C*. (*E*) Recording depth vs. power ratio for currents recorded at different holding potentials.

oscillation is mediated exclusively by excitatory inputs. The reduction of the peak at ≈2 Hz and the overall increase in power at high frequencies are similar to those found in L2/3 neurons, indicating that the synaptic inputs underlying the slow spontaneous activity are similar across layers.

To summarize the effect of membrane potential on the temporal pattern of spontaneous currents, we plotted the cortical depth against the power ratio of each cell for each of the holding potentials: −100, −70, −40, and 0 mV (Fig. 4*E*). Although the power ratio depended strongly on cortical depth at −100 mV and −70 mV ($P < 0.0025$), the dependence was weaker at −40 mV ($P < 0.01$) and insignificant at 0 mV ($P > 0.1$). This finding further supports the notion that the distinct patterns of spontaneous activity in different layers are largely attributable to excitatory inputs.

**Spatiotemporal RFs of Fast and Slow Oscillating Cells.** Does the layer-specific spontaneous oscillation play any role in visual coding? To address this question, we measured the responses of both L2/3 and L5 pyramidal neurons to visual stimuli. Sparse noise was presented, in which a bright square was flashed on a dark background at each of the 7 × 7 positions in a pseudorandom sequence (Fig. 5*A*). Synaptic currents were recorded under voltage clamp at −70 mV, which consists primarily of excitatory synaptic inputs. We found a strong similarity between the temporal patterns of visually evoked and spontaneous synaptic activity. Layer 2/3 neurons with slow spontaneous activity exhibited low-frequency, sustained current events during visual stimulation (Fig. 5*B*), whereas L5 neurons with fast spontaneous oscillations showed high-frequency, transient responses (Fig. 5*E*). We then computed the spatiotemporal RF from these current responses using reverse correlation (22), and the result was presented either as the temporal responses at different pixels (Fig. 5 *C* and *F*) or as the spatial RF profile at different time delays (Fig. 5 *D* and *G*). We found that most of the slow oscillating cells showed significant responses within the RF for a period well over 100 ms (Fig. 5 *C* and *D*), but the responses of the fast-oscillating neurons were much more transient (Fig. 5 *F* and *G*). Thus, the layer-specific temporal patterns of ongoing synaptic inputs are directly reflected in the time course of the neuronal RF.

To quantify the spatiotemporal RF properties, we fitted the spatial profile at each temporal delay with a 2-D Gaussian function to determine the RF size (Fig. 6*A Lower*, elliptical contour). The response amplitude as a function of time (*Upper*) was used to determine the time of peak and the duration of the response (see *Materials and Methods*). We then analyzed the relationship between each RF parameter and the power ratio characterizing the spontaneous activity. As shown in Fig. 6*B*, we found a strong correlation between the RF duration and the power ratio ($P < 0.002$), with fast-oscillating cells (high power ratio) exhibiting shorter RF durations. This finding is consistent with our observation that the spontaneous and visually evoked synaptic inputs exhibit similar temporal characteristics (Fig. 5). Interestingly, we also found a significant correlation between the RF size at the time of peak (Fig. 6*A*) and the spontaneous power ratio, with the slow oscillating cells showing larger RFs (Fig. 6*C*, see *Discussion*). Because the RF size and duration directly reflect the spatial and temporal windows of visual integration in neuronal responses, the above finding indicates that the spatiotemporal scale of visual representation is closely related to the temporal pattern of spontaneous activity in each layer. Similar differences between L5 and L2/3 neurons in RF duration and size were observed under urethane anesthesia (Fig. S3).

**Excitatory and Inhibitory RFs.** Because the recordings were made at −70 mV, the RF measured in the above experiment was approximately the RF of the excitatory input. For a subset of the cells, we

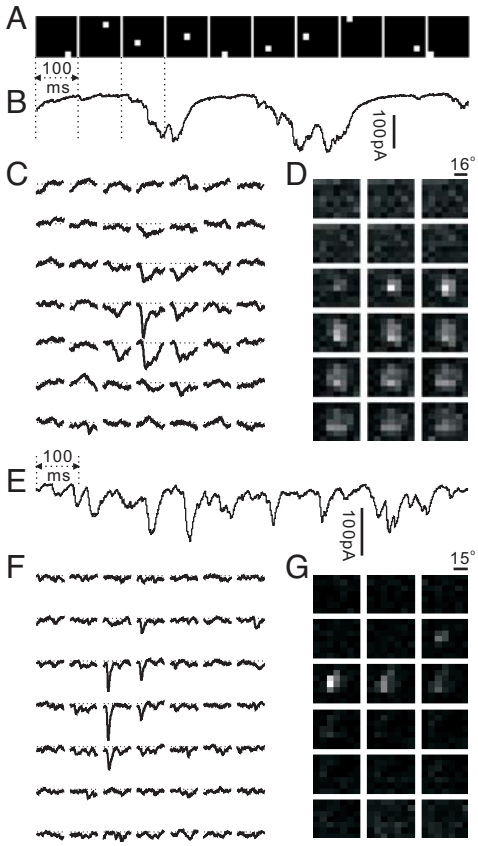


**Fig. 5.** Spatiotemporal RFs of L2/3 and L5 neurons. (*A*) A segment of sparse noise sequence. (*B*) Synaptic current recorded during the stimulus in *A* from a L2/3 neuron. (*C*) Representation of spatiotemporal RF as average current responses in different pixels, shown on the same scale as *B*; duration of each trace is 200 ms. Dashed line, current level at resting state. (*D*) Representation of spatiotemporal RF as spatial RF profile at different time delays (10 ms/frame). (*E–G*) Same as *B–D* for a L5 pyramidal neuron.

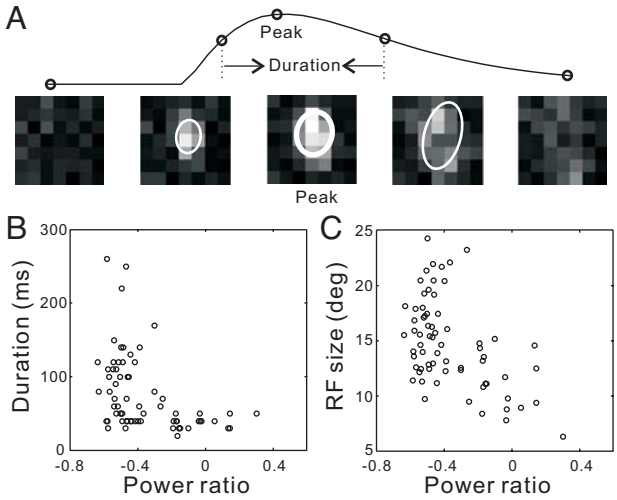


**Fig. 6.** Relationship between spatiotemporal RF properties and spontaneous activity pattern. (*A*) Illustration of parameter fitting of spatiotemporal RF. Spatial RF in each frame was fitted with 2-D Gaussian (*Lower*, white ellipse). Shown are spatial RF profiles at five temporal delays (circles in *Upper* trace). The third frame shown is the RF at the time of peak response; diameter of ellipse (geometric mean of long and short axes) is plotted in *C*. Amplitude of Gaussian fit is plotted against time (*Upper* trace) to obtain the time of peak and RF duration. (*B*) Response duration vs. spontaneous power ratio. The correlation is significant ($P < 0.002$). (*C*) RF size vs. power ratio. The correlation is significant ($P < 0.0003$).

also assessed the RFs of the inhibitory inputs. We recorded the responses of each cell to the sparse noise stimuli (Fig. 5*A*) at multiple holding potentials and estimated the excitatory and inhibitory conductance changes evoked by these stimuli (23) (see *Materials and Methods*). Note that given the poor voltage control at distal dendrites (Fig. 4*A*), the above method provides only rough estimates of the synaptic conductance. The spatiotemporal RF of each conductance was then computed by reverse correlation (22). For L2/3 cells, the inhibitory RF showed a slower onset and longer duration than the excitatory RF (Fig. 7*A*), consistent with the finding in auditory (23) and somatosensory (24) cortex. For some L5 neurons, the inhibitory RF also showed slower onset and longer duration than the excitatory RF, similar to that observed in L2/3 neurons. In other neurons, however, we observed two components of the inhibitory RF: an early component with similar onset to that of the excitatory RF, and a late component occurring ≈150 ms after the early component (Fig. 7*B*). Thus, the temporal structures of inhibitory RFs of L5 pyramidal neurons are more complex and variable across cells.

## Discussion

In this study, we used in vivo whole-cell recordings to measure the spontaneous oscillations and spatiotemporal RF properties of cortical pyramidal neurons. There are several advantages of this technique. First, it measures subthreshold synaptic inputs, which is crucial for revealing the oscillatory activity patterns given the low spontaneous firing rate of these cortical neurons. Second, it allows estimation of the excitatory and inhibitory inputs to each cell, which cannot be achieved by single-unit or LFP recordings. Finally, it allows labeling and reconstruction of the recorded neurons to determine their morphology and laminar location. Based on such a combination of information, we showed that the temporal patterns of ongoing excitatory synaptic activity are layer specific. Moreover, the spontaneous oscillations are closely related to both the spatial and temporal RF properties, indicating that the temporal dynamics of the local network play important roles in shaping the neural code in each cortical layer.

**Layer-Specific Network Oscillation.** The large amplitudes of the spontaneous synaptic currents recorded in both L2/3 (Fig. 1) and L5 (Fig. 2) indicate that they result from correlated spiking of multiple presynaptic neurons. Thus, although whole-cell recording was made from one neuron at a time, it allowed us to monitor synchronous network activity. Previous studies in somatosensory cortical slices

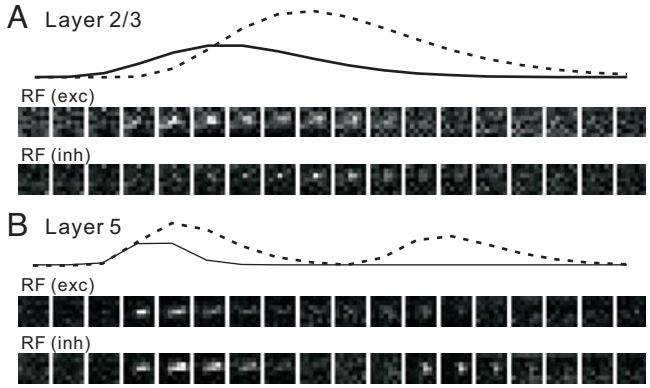


**Fig. 7.** Excitatory and inhibitory RFs of L2/3 and L5 neurons. (*A*) Excitatory and inhibitory RFs of a L2/3 neuron (20 ms/frame). Traces above show time course of the RFs (solid line, excitatory; dashed line, inhibitory). (*B*) Excitatory and inhibitory RFs of a L5 neuron (solid line, excitatory; dashed line, inhibitory).

have revealed two types of synchronous oscillations: 1–5-Hz oscillation generated in L2/3 and 8–12-Hz oscillation generated in L5 (25, 26). Although these oscillations were often induced pharmacologically in slices, their similarity to the ongoing oscillations we have observed in vivo in terms of frequency and laminar distribution strongly suggest shared mechanisms. The L5 oscillation is thought to arise from the intrinsic membrane properties of individual pyramidal neurons, since >50% of L5 pyramidal neurons are prone to rhythmic firing at 5–12 Hz, a pattern that depends on $Na^+$ channels and $Ca^{2+}$-dependent conductances (25). Our finding that the L5 oscillation at 10–15 Hz is mediated exclusively by excitatory synaptic inputs (Fig. 4) is consistent with the notion that these inputs originate from rhythmically firing pyramidal neurons. This phenomenon is is different from gamma oscillation, which depends critically on the activity of inhibitory interneurons (17–20).

To understand the function of oscillations in coding sensory information (6–9) and in gating neuronal interactions (10), most previous studies have focused on the synchronization of oscillations along the cortical surface (4–6, 13). However, a recent study in the visual cortex of awake monkeys has indicated the existence of layer-specific attention modulation of oscillations (27). Our study shows that at least two distinct types of oscillations can coexist in different layers of the visual cortex. It would be interesting for future studies to determine whether and how each type of oscillation is modulated by attention or behavior in awake animals.

**Layer-Specific RF Properties.** Changes in RF properties across layers have been analyzed in visual (28–30), auditory (31), and somatosensory (32, 33) cortical areas. In cat visual cortex, the spatial RF structure, the temporal response characteristics, and simple/complex cell classification have all been shown to depend on the laminar location, with the most salient differences found between the layers receiving direct thalamic inputs (4 and 6) and other layers (2/3 and 5) (28–30, 34). In this study, we did not find any labeled neurons in layer 4 or 6, probably due to their smaller cell bodies or greater cortical depth. This lack of sampling prevented us from analyzing the spontaneous activity and RF properties in the input layers.

For L2/3 and L5 neurons, we have focused on their response duration and RF size. Interestingly, although L2/3 neurons project strongly to L5 (14), the excitatory inputs to L5 neurons exhibit much more transient visual responses (Figs. 5–7). One possibility is that the spiking activity of L2/3 neurons exhibits more transient responses than their subthreshold activity, because the delayed inhibition (Fig. 7*A*) could truncate the spiking evoked by excitation within 10–20 ms, and spike frequency adaptation can further shorten the burst duration. In addition, a significant proportion of the excitatory inputs to L5 neurons may originate from other L5 neurons (16) with a propensity for high-frequency oscillations and transient responses. As shown in Fig. 4*C*, changing the holding potential at the soma has a much stronger effect on the amplitude of the fast-oscillating synaptic currents than on the slower inward currents, suggesting that the fast currents represent inputs from more proximal dendrites. This observation is consistent with previous findings in cortical slices that L5 inputs are located more proximally than L2/3 inputs (16, 35), giving the L5 inputs greater control of postsynaptic responses. In the somatosensory cortex, the sensory response is also found to be more transient in L5 than in L2/3 (36, 37), perhaps due to the same mechanism.

Regarding the RF size, previous studies in cat visual cortex suggested that L5 neurons exhibit larger RFs than L2/3 neurons (e.g., ref. 28). The discrepancy between the previous and current results may be due to species difference or the different methods for measuring RFs. While in previous studies the RF was defined as the area in which responses can be elicited by relatively constant visual stimuli (drifting gratings or moving bars), in this study we measured RF size at the peak of the response to sparse noise. We noticed that for many cells (e.g., Fig. 6*A*) the RF size expands considerably over several tens of milliseconds after response onset, and for L5 neurons the RFs have less time for expansion due to the shorter response duration. Thus, the effective RF size is likely to depend on the temporal properties of the visual stimuli.

**Relationship Between Spontaneous and Evoked Activity.** Spontaneous activity is known to exert powerful influences on sensory evoked responses (38, 39), causing large trial-to-trial variability through linear (40) or nonlinear (41, 42) interactions. Our study has revealed a different type of relationship between the spontaneous and evoked neural activity. Temporally, neurons with fast spontaneous oscillations show transient visual responses (Fig. 5 *E–G*). This effect may be because the L5 pyramidal neurons providing excitatory inputs to the recorded cell are entrained to fire only during certain phases of the 10–15-Hz oscillation, preferentially relaying and boosting the visual responses that arrive in phase with the oscillation. Thus, the ongoing oscillation may serve as a clock that sets the temporal window for visual integration. Spatially, the fast-oscillating neurons have smaller RFs, indicating less spatial integration. In addition to the shorter response duration, the spatial extent of network synchronization is in general negatively correlated with the oscillation frequency (43). The faster oscillation in L5 is likely to be temporally coherent across fewer cortical columns, which may result in less spatial integration among cortical neurons (10).

Together, our findings suggest that ongoing network oscillations can serve to gate sensory inputs, with fast-oscillating circuits preserving both spatial and temporal specificity and slow oscillating networks integrating over longer time and across larger space. Different cortical layers exhibit distinct projection patterns, with L2/3 sending its output to higher cortical areas for further visual feature analyses, and L5 projecting strongly to the superior colliculus involved in controlling eye movement (14). The different types of visual signals represented in these layers, shaped by local network dynamics, may be specifically suited for the functions of their downstream neural circuits.

## Materials and Methods

**Surgery and Preparation.** All procedures were approved by the Animal Care and Use Committee at University of California Berkeley. Adult Long-Evans rats (p60–p90) were anesthetized with pentobarbital (Nembutal, initial dose 40 mg/kg, maintained at 7.5 mg/h, supplemented as needed, i.p.) or urethane (1.2–.5 g/kg, given in two half-doses with 20–30 min in between) and restrained in a stereotaxic apparatus (David Kopf Instruments). Body temperature was maintained at 37.5 °C via a heating pad. Craniotomy (diameter 0.6 mm) was made above the monocular region of right V1, and dura was removed. The left eye was fixed with a metal ring to prevent eye movement and irrigated with sterile saline. At the end of experiment, animals were euthanized with overdose of pentobarbital sodium. For histological reconstruction, the animal was immediately perfused with chilled 4% formaldehyde solution in 0.1 M PBS, and the brain was removed and fixed in the formaldehyde solution overnight at 4 °C.

**Recordings.** All recordings were made with an Axopatch 700B amplifier (Axon Instruments). Patch pipettes (2–5 MΩ) were filled with internal solution containing (in mM) K-gluconate 120, KCl 10, MgCl 1, phosphocreatine 10, MgATP 4, GTP 0.5, Hepes 10, and EGTA 0.1. For perforated patch, amphotericin B (0.5 mg/mL, EMD Biosciences) was added. In conventional whole-cell recordings for histological staining, neurobiotin (0.5%) was added in the internal solution; to estimate excitatory and inhibitory inputs (Figs. 4 and 7), QX-314 (10 mM, EMD Biosciences) was added to block voltage-sensitive $Na^+$ channels. Data were filtered at 2 kHz, sampled at 10 kHz by an Axon 1200 acquisition board (Axon Instruments), and analyzed with custom software in Matlab. Mean resting potential of the cells was $-71.3 \pm 4.9$ mV (before correcting for liquid junction potential of ≈10 mV). With conventional whole-cell recording, series resistance was 34.5–76.5 MΩ (54.1 ± 13.3 MΩ, mean ± SD). LFP recording was made with patch electrode (2–5 MΩ, filled with saline) and band-pass filtered (low cutoff, 0.1 Hz; high cutoff, 400–800 Hz).

**Visual Stimulation.** Visual stimuli were presented with a mini-LCD monitor (87 × 155 mm; Xenarc Technologies Corp.; refresh rate 60 Hz; maximal luminance 350 cd/m$^2$) placed 35 mm from the left eye. RFs were mapped with sparse noise, with

a bright square ($6.5 \times 6.5^{\circ} - 10.2 \times 10.2^{\circ}$) flashing on black background at each of the $7 \times 7$ positions in a pseudorandom sequence (25 flashes/position). Stimulus was updated every 6 or 12 frames, resulting in an effective frame rate of 10 or 5 Hz, respectively.

**Histological Staining.** After fixation, the brain was washed in PBS three times, 15 min each. The V1 area containing the recorded cell was cut using a vibratome (Serial 1000 Tissue Sectioning System; Ted Pella Inc.) into 350-$\mu$m-thick slices and incubated in streptavidin-FITC (1:1,000) overnight. Slices were mounted with Vectorshield (Vector Laboratories), and the coverslip was sealed with nail polish. Images were collected with a Leica confocal microscope with a 40× Plan Apo objective (NA 1.0).

**Data Analysis.** Power spectrum of spontaneous activity was computed from 0.5–5 min of continuous recordings (≈2 min for most cells).

**Estimation of Excitatory and Inhibitory Inputs.** For each sparse noise sequence, current responses were recorded at three or four holding potentials (−100 to +20 mV). The procedure for estimating excitatory and inhibitory conductances is similar to that used in a previous study (23). Briefly, at each moment of the stimulus sequence, the measured current was plotted against holding voltage (corrected for both liquid junction potential and voltage drop across the series resistance). Total conductance $G_T$ was measured by slope of the linear fit, and the intercept provided estimated reversal potential $E_T$. The excitatory and inhibitory conductances ($G_E$ and $G_I$) are computed as:

$$G_E(t) = G_T(t)*(E_T(t) - E_I)/(E_E - E_I) - G_R*(E_R - E_I)/(E_E - E_I) \quad [1]$$

$$G_I(t) = G_T(t)*(E_E - E_T(t))/(E_E - E_I) - G_R*(E_E - E_R)/(E_E - E_I) \quad [2]$$

where $E_E$ and $E_I$ are reversal potentials for excitatory and inhibitory conductances, respectively, $E_R$ is resting reversal potential, and $G_R$ is resting conductance. For computing the excitatory and inhibitory RFs, the term containing $G_R$ is constant and therefore does not affect RF estimation.

**RF Fitting.** To extract the spatiotemporal RF parameters, the RF $K(x, y, t)$ at each temporal frame $t$ was fitted with a 2-D Gaussian:

$$K(x, y) = Ce^{-(x'^2/\sigma_x^2 + y'^2/\sigma_y^2)} \quad [3]$$

$$x' = (x - x_0)\cos\theta + (y - y_0)\sin\theta \quad [4]$$

$$y' = -(x - x_0)\sin\theta + (y - y_0)\cos\theta \quad [5]$$

where $C$ is amplitude of the RF response, $\sigma_x$ and $\sigma_y$ determine the RF width and length, $\theta$ is orientation. RF size is measured at the time of peak response by $2(\sigma_x\sigma_y)^{1/2}$.

To obtain the temporal parameters, $C(t)$ is fitted with the probability function for gamma distribution:

$$C(t) = \begin{cases} A(t - t_0)^{\alpha}e^{-(t - t_0)/\tau} + C_0, & t > t_0 \\ C_0, & t \le t_0 \end{cases} \quad [6]$$

where $A$, $\alpha$, $\tau$, $t_0$, and $C_0$ are free parameters. The duration of visual response is measured by width at half-height of the curve (Fig. 6*A*).

**ACKNOWLEDGMENTS.** This work was supported by a grant from the National Institutes of Health National Eye Institute.

1. Kahana MJ (2006) The cognitive correlates of human brain oscillations. *J Neurosci* 26:1669–1672.
2. Buzsaki G (2002) Theta oscillations in the hippocampus. *Neuron* 33:325–340.
3. Herculano-Houzel S, Munk MH, Neuenschwander S, Singer W (1999) Precisely synchronized oscillatory firing patterns require electroencephalographic activation. *J Neurosci* 19:3992–4010.
4. Steriade M, Amzica F, Contreras D (1996) Synchronization of fast (30–40 Hz) spontaneous cortical rhythms during brain activation. *J Neurosci* 16:392–417.
5. Fries P, Reynolds JH, Rorie AE, Desimone R (2001) Modulation of oscillatory neuronal synchronization by selective visual attention. *Science* 291:1560–1563.
6. Singer W, Gray CM (1995) Visual feature integration and the temporal correlation hypothesis. *Annu Rev Neurosci* 18:555–586.
7. Wehr M, Laurent G (1996) Odour encoding by temporal sequences of firing in oscillating neural assemblies. *Nature* 384:162–166.
8. Hopfield JJ (1995) Pattern recognition computation using action potential timing for stimulus representation. *Nature* 376:33–36.
9. O'Keefe J, Recce ML (1993) Phase relationship between hippocampal place units and the EEG theta rhythm. *Hippocampus* 3:317–330.
10. Womelsdorf T, et al. (2007) Modulation of neuronal interactions through neuronal synchronization. *Science* 316:1609–1612.
11. Sejnowski TJ, Paulsen O (2006) Network oscillations: Emerging computational principles. *J Neurosci* 26:1673–1676.
12. Wespatat V, Tennigkeit F, Singer W (2004) Phase sensitivity of synaptic modifications in oscillating cells of rat visual cortex. *J Neurosci* 24:9067–9075.
13. Rodriguez E, et al. (1999) Perception's shadow: Long-distance synchronization of human brain activity. *Nature* 397:430–433.
14. Callaway EM (1998) Local circuits in primary visual cortex of the macaque monkey. *Annu Rev Neurosci* 21:47–74.
15. Hirsch JA, Martinez LM (2006) Laminar processing in the visual cortical column. *Curr Opin Neurobiol* 16:377–384.
16. Markram H (1997) A network of tufted layer 5 pyramidal neurons. *Cereb Cortex* 7:523–533.
17. Traub RD, Bibbig A, LeBeau FE, Buhl EH, Whittington MA (2004) Cellular mechanisms of neuronal population oscillations in the hippocampus in vitro. *Annu Rev Neurosci* 27:247–278.
18. Deans MR, Gibson JR, Sellitto C, Connors BW, Paul DL (2001) Synchronous activity of inhibitory networks in neocortex requires electrical synapses containing connexin36. *Neuron* 31:477–485.
19. Galarreta M, Hestrin S (1999) A network of fast-spiking cells in the neocortex connected by electrical synapses. *Nature* 402:72–75.
20. Hasenstaub A, et al. (2005) Inhibitory postsynaptic potentials carry synchronized frequency information in active cortical networks. *Neuron* 47:423–435.
21. Jonas P, Bischofberger J, Fricker D, Miles R (2004) Interneuron Diversity series: Fast in, fast out—temporal and spatial signal processing in hippocampal interneurons. *Trends Neurosci* 27:30–40.
22. Jones JP, Palmer LA (1987) The two-dimensional spatial structure of simple receptive fields in cat striate cortex. *J Neurophysiol* 58:1187–1211.
23. Wehr M, Zador AM (2003) Balanced inhibition underlies tuning and sharpens spike timing in auditory cortex. *Nature* 426:442–446.
24. Moore CI, Nelson SB (1998) Spatio-temporal subthreshold receptive fields in the vibrissa representation of rat primary somatosensory cortex. *J Neurophysiol* 80:2882–2892.
25. Silva LR, Amitai Y, Connors BW (1991) Intrinsic oscillations of neocortex generated by layer 5 pyramidal neurons. *Science* 251:432–435.
26. Flint AC, Connors BW (1996) Two types of network oscillations in neocortex mediated by distinct glutamate receptor subtypes and neuronal populations. *J Neurophysiol* 75:951–957.
27. Buffalo EA, Fries P, Desimone R (2004) Layer-specific attentional modulation in early visual areas. *Soc Neurosci Abstr* 30:717.716.
28. Gilbert CD (1977) Laminar differences in receptive field properties of cells in cat primary visual cortex. *J Physiol* 268:391–421.
29. Martinez LM, et al. (2005) Receptive field structure varies with layer in the primary visual cortex. *Nat Neurosci* 8:372–379.
30. Martinez LM, Alonso JM, Reid RC, Hirsch JA (2002) Laminar processing of stimulus orientation in cat visual cortex. *J Physiol* 540:321–333.
31. Linden JF, Schreiner CE (2003) Columnar transformations in auditory cortex? A comparison to visual and somatosensory cortices. *Cereb Cortex* 13:83–89.
32. Brecht M, Roth A, Sakmann B (2003) Dynamic receptive fields of reconstructed pyramidal cells in layers 3 and 2 of rat somatosensory barrel cortex. *J Physiol* 553:243–265.
33. Manns ID, Sakmann B, Brecht M (2004) Sub- and suprathreshold receptive field properties of pyramidal neurones in layers 5A and 5B of rat somatosensory barrel cortex. *J Physiol* 556:601–622.
34. Hirsch JA, et al. (2002) Synaptic physiology of the flow of information in the cat's visual cortex in vivo. *J Physiol* 540:335–350.
35. Sjostrom PJ, Hausser M (2006) A cooperative switch determines the sign of synaptic plasticity in distal dendrites of neocortical pyramidal neurons. *Neuron* 51:227–238.
36. Brumberg JC, Pinto DJ, Simons DJ (1999) Cortical columnar processing in the rat whisker-to-barrel system. *J Neurophysiol* 82:1808–1817.
37. Wilent WB, Contreras D (2004) Synaptic responses to whisker deflections in rat barrel cortex as a function of cortical layer and stimulus intensity. *J Neurosci* 24:3985–3998.
38. Azouz R, Gray CM (1999) Cellular mechanisms contributing to response variability of cortical neurons in vivo. *J Neurosci* 19:2209–2223.
39. Fiser J, Chiu C, Weliky M (2004) Small modulation of ongoing cortical dynamics by sensory input during natural vision. *Nature* 431:573–578.
40. Arieli A, Sterkin A, Grinvald A, Aertsen A (1996) Dynamics of ongoing activity: Explanation of the large variability in evoked cortical responses. *Science* 273:1868–1871.
41. Kisley MA, Gerstein GL (1999) Trial-to-trial variability and state-dependent modulation of auditory-evoked responses in cortex. *J Neurosci* 19:10451–10460.
42. Petersen CC, Hahn TT, Mehta M, Grinvald A, Sakmann B (2003) Interaction of sensory responses with spontaneous depolarization in layer 2/3 barrel cortex. *Proc Natl Acad Sci USA* 100:13638–13643.
43. Bullock TH, McClune MC (1989) Lateral coherence of the electrocorticogram: A new measure of brain synchrony. *Electroencephalogr Clin Neurophysiol* 73:479–498.